



Reference temperature correction and dimensionless number analysis for heat transfer of supercritical CO₂ in horizontal tubes

Zheng Wang, Gang Xiao*, Yafei Liu, Yuxuan Ji, Haoran Xu

State Key Laboratory of Clean Energy Utilization, Zhejiang University, 38 Zheda Road, Hangzhou 310027, China

ARTICLE INFO

Article history:

Received 17 February 2022

Revised 20 April 2022

Accepted 25 April 2022

Available online 7 May 2022

Keywords:

Supercritical CO₂

Heat transfer

Reference temperature

Dimensionless number

Nusselt correlation

ABSTRACT

Researchers have extensively studied convective heat transfer of variable property fluids in tubes because of their different heat transfer characteristics to constant property fluids. However, the heat transfer correlations are often limited to small or large tubes or other limited conditions when the properties of fluids change dramatically, which may be due to inaccuracy definition of the reference temperature in average heat transfer coefficient (HTC) and incorrect understanding of dimensionless parameters in Nusselt correlation.

As a typical case, this study numerically investigates the cooling heat transfer of sCO₂ in horizontal tubes near the pseudo-critical point. Eight numerical models are compared with experimental results in the literature, and the Realizable $k-\epsilon$ model with enhanced wall treatment is best for predicting cooling HTC. A new definition of reference temperature for average HTC is proposed, which is more accurate than the traditional arithmetical average of inlet and outlet bulk temperature. Sensitivity analysis of HTC is carried out for heat transfer mechanisms. In addition, the definitions of dimensionless numbers in Nusselt correlation are analyzed, and more accurate definitions are proposed. Based on the conclusions, a newly developed Nusselt correlation with concise form shows excellent results with a Root Mean Square (RMS) error of 2.9% for 6.22 and 9.40 mm tubes. It can still maintain high accuracy when it is extrapolated to 4.15 and 14 mm tubes. The numerically derived correlation agrees well with the experimental results for 2–6 mm tubes in literature and can also be extrapolated to constant property cases.

© 2022 Elsevier Ltd. All rights reserved.

1. Introduction

In the early 20th century, the supercritical carbon dioxide (sCO₂) Brayton cycle combined with the fourth generation of nuclear power plants came into our view [1]. With the characteristics of high power density, high cycle efficiency, low corrosion as opposed to the ultra-supercritical steam Rankine cycle, sCO₂ Brayton cycle can be well applied in many other fields such as fossil fuel energy [2,3], concentrated solar power [4], ship propulsion system [5] and fuel cell [6], etc. In a sCO₂ Brayton cycle, the compressor will be running near the pseudo-critical regime to obtain a high cycle efficiency [7]. Therefore, the cooling HTC is very important for precooler designing and developing sCO₂ dynamic simulation models.

However, it is difficult to predict the heat transfer of sCO₂ near pseudo-critical point for a wide range of conditions due to drastic change in its thermal physical properties, which is entirely dif-

ferent from constant property fluids [8]. Thus, researchers have conducted many experimental studies for the heat transfer characteristics under specific conditions. Yoon et al. [9] investigated sCO₂ cooling heat transfer in 7.73 mm horizontal circular tube under uniform heat flux boundary with Reynolds number (Re) of 3×10^4 – 1.8×10^5 . The previous correlations generally underestimate the HTC of sCO₂ in the pseudo-critical regime compared to their experimental result. They concluded that the contribution of wall and bulk fluid to supercritical heat transfer is different. Therefore, a new Nusselt correlation based on Baskov's correlation with the dimensionless isobaric specific heat and density correction terms was developed, which could predict most of their experimental results with the error less than $\pm 20\%$, though a few points deviated significantly from their new correlations. Liao and Zhao [10] investigated sCO₂ cooling heat transfer in 0.5–2.16 mm horizontal circular tube under constant temperature boundary with the Re up to 10^5 . They found that the HTC of the large-diameter tube was higher than that of the small-diameter tube due to the stronger secondary flow caused by the buoyancy effect. Therefore, they used the Richardson number to represent the strength of buoyancy, and obtained a well-applicable correlation worked in

* Corresponding author.

E-mail address: xiaogangtianmen@zju.edu.cn (G. Xiao).

tube diameters of 0.5–2.16 mm with another two additional terms of dimensionless isobaric specific heat and density. Dang and Hihara [11] investigated sCO_2 cooling heat transfer in 1–6 mm horizontal circular tube under uniform heat flux boundary with the Re of 2×10^4 – 1.5×10^5 at different pressures, mass flow rates and heat flux. They analyzed the heat transfer process qualitatively and concluded that the thermal resistance is mainly concentrated in the viscous sublayer, so the thermal conductivity and friction factor should be evaluated at film temperature. A new Nusselt correlation based on Gnielinski correlation was developed to divide the pseudo-critical regime into three regions, which agrees with experimental results but with a complex form and lots of branching conditions. Huai et al. [12] investigated sCO_2 cooling heat transfer in 1.13 mm multi-port circular mini channels with the Re of 2×10^3 – 2.6×10^4 . The HTC measured in their experiments were significantly lower than those in the literature. Based on the Dittus-Boelter (DB) correlation, a new correlation with the isobaric specific heat and density correction terms was developed. However, the maximum error reached $\pm 30\%$, perhaps because the original form of DB correlation was not suitable for the supercritical heat transfer process. Oh and Son [13] investigated cooling heat transfer of sCO_2 in 4.55/7.75 mm macro-tubes under uniform heat flux boundary with the Re of 2×10^4 – 1.3×10^5 . They compared many correlations with their experimental results and found that most correlations showed a significant deviation. They divided supercritical heat transfer into two regions based on pseudo-critical points. A new Nusselt correlation was developed with dimensionless isobaric specific heat and dimensionless density. However, it still needs to be further confirmed for the large discrepancy with others, which Fang and Xu [14] and Wang et al. [15] also announced. Liu et al. [16] investigated cooling heat transfer in 4–10.7 mm horizontal circular tube under uniform heat flux boundary with the Re of 1×10^4 – 1.6×10^5 . They found that noticeable deviation would occur when the correlation for small tubes is applied to large tubes. Based on isobaric specific heat and density correction terms, they developed a well-fitting Nusselt correlation with the reference temperature of the wall. Wahl et al. [17] studied local cooling heat transfer coefficient in 2 mm horizontal circular tube with the Re of 1×10^4 – 1.6×10^5 . They found that when the mass flow rate was reasonably high, the existing correlation failed in predicting the experimental results. Based on the reference temperature of the wall and regime of over pseudocritical or under pseudocritical, they developed a complex correlation with four property correction terms and successfully predicted most of their experimental results. By summarizing the researchers' work, it is found that the experimental conditions of most researchers are relatively narrow. Therefore, when the correlation is applied to other conditions, especially under larger or smaller pipes, failure in prediction would occur. In addition, many researchers do not discuss the influence of heat flux on HTC, but it is an essential factor affecting supercritical heat transfer.

Most experiment-based sCO_2 cooling heat transfer Nusselt correlations were developed based on tube diameters less than 10.7 mm and Re within 2×10^5 . Moreover, some of them have a very complex form with many correction terms, which are difficult to extrapolate, although they worked well within a limited range of conditions. In fact, for experimental study, another significant concern is that the introduction of lubricating oil by mechanical supercharging equipment would also inevitably occur, which would deteriorate the heat transfer of sCO_2 [18–21]. Most researchers did not claim that they have installed oil separators in their experiment loop, so the reliability of many experimental results still needs further consideration and examination.

In recent decades, with the development of computers, numerical simulation has gradually become an effective way to study sCO_2 heat transfer characteristics. Dang and Hihara [22] numer-

ically investigated sCO_2 cooling heat transfer in 6mm horizontal tube and heating heat transfer in 10 mm horizontal tube and found that the JL k - ε model well predicted the experiment results. Jiang et al. [23] numerically studied sCO_2 heating heat transfer in 0.27 mm vertical tube for buoyancy and flow acceleration effect. The realizable k - ε model shows better agreement with their experiment data. Wang et al. [24] numerically investigated buoyancy effect and buoyancy criterion of sCO_2 in helically coiled tubes under heating conditions. They found that the SST k - ω model gives better predictions due to accurate flow separation capturing. Zhang et al. [25,26], Guo et al. [27] also confirmed that SST k - ω is an accurate sCO_2 heat transfer prediction model. Du et al. [28] compared nine numerical models in predicting cooling heat transfer of sCO_2 and found that the LB k - ε model shows the best agreement with the experiment data, which was also announced by Diao et al. [29] and Zhao et al. [30]. Wang et al. [31] numerically investigated cooling heat transfer in 15.75–24.36 mm horizontal tubes. They found that the AKN k - ε model was effective in large diameter tubes. The numerical results concluded that buoyancy in large diameter tubes would deteriorate heat transfer. They also used the AKN k - ε model to derive the Nusselt correlation of sCO_2 cooling heat transfer [15]. Overall, many researchers have used numerical simulation to study the heat transfer process of sCO_2 , and most of them are focused on the buoyancy effect and heat transfer deterioration near pseudo-critical points. Due to the advantages of numerical simulation in predicting the distribution of physical parameters in the flow field, more in-depth conclusions can be obtained by analyzing the heat transfer process through numerical results. It is worth noting that only turbulence models with near-wall solutions can successfully capture sCO_2 heat transfer characteristics near pseudo-critical points.

A remarkable fact is that, for the experimental study of supercritical cooling heat transfer, it is difficult to determine the local HTC because of the difficulty in measuring local heat flux [32]. Huai et al. [12] measured the local heat flux by setting heat flux sensors around the tube, but the measurement accuracy is affected by the contact tightness between the sensor and the tube. Jiang et al. [32] combined the simulation method with the experimental results. They calculated the enthalpy change of water by taking the measured temperature of the tube wall as the input boundary of the simulation to determine the local heat flux. Wahl et al. [17] used the discretization method to calculate the heat flux by assuming that the HTC on the cooling water side was constant. However, complex measurement means or simulation or calculation methods may bring additional errors to the results. In contrast, measuring average HTC is relatively simple and feasible. However, when calculating the average heat transfer coefficient, the widely used method to define the reference temperature is arithmetic average inlet and outlet temperature, which need to be further examined when used for variable property fluids. The temperature profile along the flow direction will deviate from a straight line compared to constant property fluids, which will be more evident when heat flux to mass flux is large. In addition, to our knowledge, few researchers have analyzed and discussed the form of Nusselt correlation for variable property fluids in detail. Therefore, the correct form of Nusselt correlation of variable property fluids also needs to be investigated.

Based on the above deficiencies, this paper adopts numerical methods to simulate and analyze the cooling heat transfer of sCO_2 in horizontal tubes near the pseudo-critical regime. The accuracy of eight numerical models is compared and analyzed. The reference temperature definition of average HTC is investigated, and a new definition is proposed. The dimensionless parameters of the Nusselt correlation are further discussed. Finally, a new widely applicable Nusselt correlation is proposed.

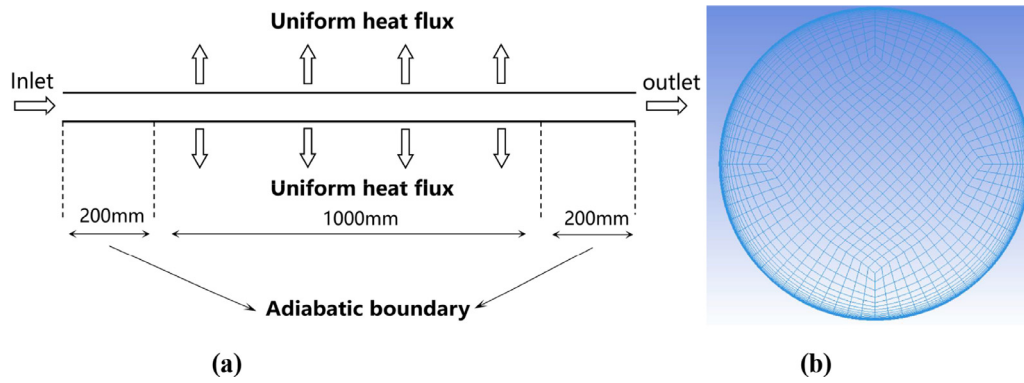


Fig. 1. (a) Schematic of the physical model; (b) Cross-section of the grid.

2. Numerical model validation

2.1. Physical model and boundary condition

This work numerically studied the near pseudo-critical regime cooling heat transfer of sCO₂ in horizontal circular tubes by ANSYS fluent. Considering it has been widely recognized that the boundary condition of counterflow convective heat transfer of water is almost equivalent to uniform heat flux [11,28,31], only the CO₂ domain was considered, and the thickness of the wall was ignored. The physical model is shown in Fig. 1(a).

The tube length is 1.4 m with 0.2 m adiabatic velocity developing section [33], 1.0 m uniform wall heat flux section and 0.2 m adiabatic outlet section. The inner diameter of the tube was set to 6.22 mm. The mass flow inlet and mass flow outlet were set for inlet and outlet boundary conditions, respectively. The inlet was at the axis coordinate of -0.2 m, and the outlet was at 1.2 m.

2.2. Solution setup and grid independence check

To accurately reflect the drastic change of physical properties of sCO₂ at the pseudo-critical regime and speed up the calculation, the piecewise linear function, which considers the properties as temperature-dependent, was adopted in our simulation. Some researchers have also adopted this method, but the excessive sampling interval of 1 K would lead to imprecise results when the temperature near the pseudo-critical point [34]. The Differential Evolution (DE) algorithm was adopted, which put 50 property points into the temperature range to minimize the area enclosed by the piecewise linear function and the original property curve. The properties were obtained from the NIST Refprop database 9.1 [35]. The structured mesh is generated and was split into O grid mesh in The Integrated Computer Engineering and Manufacturing code for Computational Fluid Dynamics (ICEM CFD) to improve the accuracy and speed up the calculation. To satisfy the near-wall solution, *y+* was set to less than 0.5. The cross-section of the grid is shown in Fig. 1(b).

In order to proceed with grid independence check, a method commonly used in literature for the definition of average HTC was adopted, which can be obtained by Eq. (1).

$$h(T_r) = \frac{H_{b,in} - H_{b,out}}{A_w \cdot (T_r - T_w)} \quad (1)$$

Where *T_r* is arithmetic average bulk temperature of inlet and outlet; *H_{b,in}* is inlet bulk enthalpy; *H_{b,out}* is outlet bulk enthalpy; *A_w* is heat transfer area; *T_w* is the inner average temperature of the wall. They can be further represented by Eqs. (2)–(5).

$$H_b = \frac{\iint_{A_c} \rho u H dA_c}{\iint_{A_c} \rho u dA_c} \quad (2)$$

$$T_b = T(H_b, P) \quad (3)$$

$$T_r = \frac{T_{b,in} + T_{b,out}}{2} \quad (4)$$

$$T_w = \frac{\iint_{A_w} T_{w,local} dA_w}{A_w} \quad (5)$$

Where *ρ* represents local density; *u* represents local axial velocity; *H* represents local enthalpy; *A_c* represents flow cross-section area; *P* represents pressure; *T_{w,local}* represents the local temperature of the wall. *T_b* is the function of enthalpy and pressure, which can be calculated from the NIST Refprop database 9.1 [35].

The boundary conditions for grid independence check were set to the pressure of 7.8 MPa, the mass flux of 657.6 kg/(m²•s) and the heat flux of 22 kW/m². Realizable *k-ε* model with enhanced wall treatment was used for grid independence check. The gravity acceleration and full buoyancy effect were introduced. Pressure based solver and Coupled method was adopted for faster convergence. All the residuals were set within 10⁻⁵. For each case, the first 150 steps used the First Order Upwind scheme to generate a preliminary physical field. The subsequent steps used the Second Order Upwind scheme to get a numerically reasonable result. For a few cases where the convergence is challenging, calculations were stopped when the outlet temperature no longer changed within 200 steps. The grid cells for grid independence check were 316,500, 826,900, 1,727,900, respectively.

The check results are shown in Fig. 2. There are almost no discrepancies for the three meshes. So mesh1 with the least cells is sufficient for solution results. Subsequent simulations of other pipe diameters also used the same grid scale as mesh1.

2.3. Comparison of numerical models

Eight numerical models have been selected for validation. Four low *Re k-ε* model namely Abid [36], AKN [37], CHC [38], LS [39]. Three enhanced wall treatment model of Standard *k-ε*, Realizable *k-ε*, RNG *k-ε*. And SST *k-ω* model. The boundary conditions are the same as that in Section 2.2. Because Dang and Hihara's [11] experimental data are widely accepted by researchers [14–17,29], their experimentally derived correlation was selected to test the average HTC results of numerical models. Taler's [40] newer developed correlation for turbulent fluid flow with uniform wall heat flux for constant property fluids is also adopted for comparison.

The results of each numerical model with the comparison of the Dittus-Boelter (DB) correlation, Dang and Hihara correlation and Taler correlation are shown in Fig. 3. It can be obtained from Fig. 3 that the traditional DB correlation significantly underestimates HTC around the pseudocritical regime. D. Taler correlation

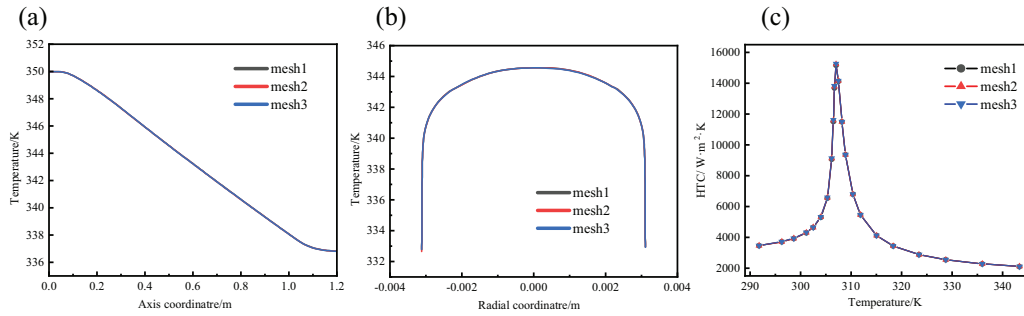


Fig. 2. Grid independence check. (a) Axis temperature; (b) Vertical radial temperature at axis coordinate of 0.5 m; (c) average HTC.

well predicted the HTC under the pseudocritical temperature but underestimated HTC above the pseudocritical point. All the numerical models can successfully predict the variation trend of HTC. Near the pseudo-critical point, only the RNG $k-\epsilon$ model could well predict the average HTC. But the RNG $k-\epsilon$ model will significantly overestimate the HTC when the temperature departs from the pseudocritical point, which is considered to be unreasonable. CHC, YS, SST $k-\omega$ would evidently underestimate average HTC. Abid can perfectly predict HTC under the pseudo-critical point but overestimate HTC when the temperature is well above the pseudo-critical point. AKN will overestimate the HTC when the temperature is well above or below the pseudocritical temperature. The Standard $k-\epsilon$ and the Realizable $k-\epsilon$ have good accuracy for predicting the HTC in the whole temperature regime. The Realizable $k-\epsilon$ model works best with a lower average relative error of 7.9% compared with the Standard $k-\epsilon$ model of 8.5%, which was also recommended by Jiang et al. [23] for heating conditions. Therefore, the Realizable $k-\epsilon$ model was chosen to continue the subsequent simulation.

3. Reference temperature of average HTC for variable property fluids

3.1. Discussion of average HTC

The HTC calculated from Eq. (1) is only the so-called ‘average HTC’ but inconsistent with the actual local HTC. When the test section is short, the average HTC could be approximately equal to local HTC. However, the thermal entrance effect would become significant, making the predicted value of average HTC higher than fully developed ones [41].

Take a straight tube for analysis. Define h_l as local HTC and h_a as average HTC. Eq. (6) can be obtained by the principle of energy conservation in a fully developed section.

$$\iint_{A_w} h_l(T_b - T_w)dA_w = h_a A_w \overline{\Delta T} \quad (6)$$

Where A_w is the inner area of the wall; h_a is the average HTC; $\overline{\Delta T}$ is the average heat transfer temperature difference.

The total heat transfer section can be divided into finite sections for approximate calculation of h_a . Eq. (7) could be derived assuming the inner wall area of each section is equal to δA .

$$h_{l1}(T_{b1} - T_{w1})\delta A + h_{l2}(T_{b2} - T_{w2})\delta A + \dots + h_{ln}(T_{bn} - T_{wn})\delta A = h_a A_w \overline{\Delta T} \quad (7)$$

Where h_{ln} is the local HTC in the n th segment; T_{bn} is the average bulk temperature of the middle cross-section of the n th segment; T_{wn} is the average wall temperature of the n th segment.

The average heat transfer temperature difference was discussed in Supplementary information chapter 1. Combining Eqs. (7) and

(S2), Eq. (8) could be derived.

$$h_a = \frac{h_{l1}(T_{b1} - T_{w1})\delta A + h_{l2}(T_{b2} - T_{w2})\delta A + \dots + h_{ln}(T_{bn} - T_{wn})\delta A}{A \frac{(T_{b1} - T_{w1}) + (T_{b2} - T_{w2}) + \dots + (T_{bn} - T_{wn})}{n}} = \frac{h_{l1}(T_{b1} - T_{w1}) + h_{l2}(T_{b2} - T_{w2}) + \dots + h_{ln}(T_{bn} - T_{wn})}{(T_{b1} - T_{w1}) + (T_{b2} - T_{w2}) + \dots + (T_{bn} - T_{wn})} \quad (8)$$

If h_a could represent local HTC, then replace h_{ln} with h_{an} . A checked local HTC named ‘ h'_a ’ could be derived as Eq. (9).

$$h'_a = \frac{h_{a1}(T_{b1} - T_{w1}) + h_{a2}(T_{b2} - T_{w2}) + \dots + h_{an}(T_{bn} - T_{wn})}{(T_{b1} - T_{w1}) + (T_{b2} - T_{w2}) + \dots + (T_{bn} - T_{wn})} \quad (9)$$

Define an error test function as Eq. (10).

$$Er = \left| \frac{h'_a - h_a}{h_a} \right| \quad (10)$$

It is evident that the smaller Er is, the closer the average HTC is to the actual local HTC.

3.2. Exclusion of thermal entrance effect

The thermal entrance effect would occur in a short inlet section, which will make the HTC much higher than that in the fully developed region [41]. Notter and Sleicher [42] concluded that the exact calculation of the thermal entrance region length is relatively complicated. However, the entrance length can be estimated by graphical results in their article. Because the Re is less than 10^6 and Prandtl number (Pr) is larger than 0.72 in this study, the thermal entrance length will result as Eq. (11).

$$\frac{\bar{x}}{D} < 15 \quad (11)$$

According to Eq. (11), \bar{x} would be less than 93.3 mm for a 6.22 mm diameter tube. Simulation results can well verify this conclusion, as shown in Fig. 4. The temperature at the central axis is not affected by the heat transfer in a short length close to the inlet section. The central temperature begins to decline at a position of about 50 mm. At 100 mm, its downward trend is almost stable, which means that the heat transfer has reached the thermally fully developed regime. So finally, 200–1000 mm was selected as the fully developed regime in our analysis.

3.3. Reference temperature of average HTC

In previous literature for calculating average HTC, researchers usually define reference temperature by an arithmetical average of inlet and outlet bulk temperature. This definition is reasonable for constant property fluids because the C_p keeps constant along the flow direction. However, this method will have problems for fluid near the pseudo-critical point. Some detailed analysis can be found in Supplementary information chapter 2.

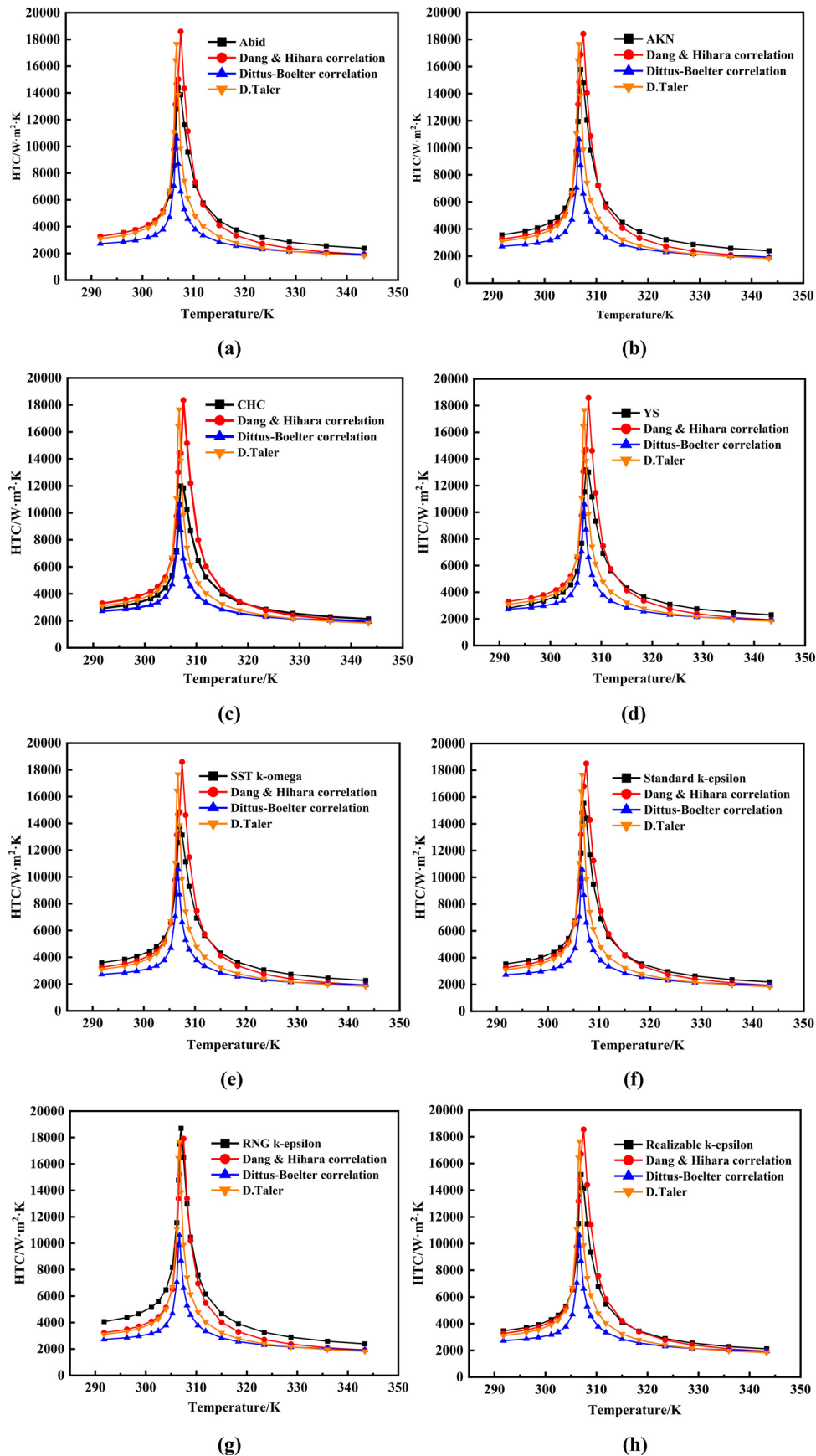


Fig. 3. Examination of numerical models. (a) Abid; (b) AKN; (c) CHC; (d) YS; (e) SST $k-\omega$; (f) Standard $k-\epsilon$; (g) RNG $k-\epsilon$; (h) Realizable $k-\epsilon$.

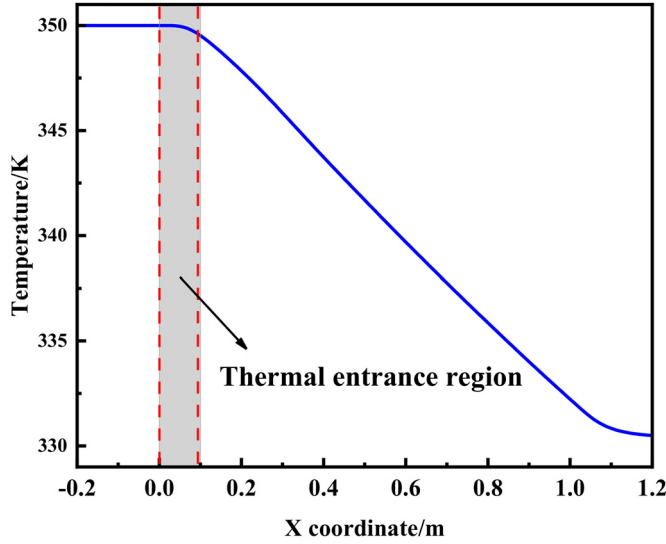


Fig. 4. The temperature of the central axis along the flow direction.

According to the conclusions in 3.1, the reference temperature of HTC can be evaluated by Eq. (10). For Eq. (9)'s calculation, 200–1000 mm section was divided into twenty segments. Consequently, Eq. (9) turned into Eq. (12).

$$h'_a = \frac{h_{a1}(T_{b1} - T_{w1}) + h_{a2}(T_{b2} - T_{w2}) + \dots + h_{a20}(T_{bn} - T_{wn})}{(T_{b1} - T_{w1}) + (T_{b2} - T_{w2}) + \dots + (T_{b20} - T_{w20})} \quad (12)$$

In order to select an appropriate reference temperature, the following four methods of calculating reference temperature were compared, which can be expressed by Eqs. (13)–(16).

Method 1 (Traditional):

$$T_b = \frac{T_{bin} + T_{bout}}{2} \quad (13)$$

Method 2:

$$T_b = \frac{T_{b1} + T_{b2} + \dots + T_{b20}}{20} \quad (14)$$

Method 3:

$$T_b = T \left(\frac{H_{bin} + H_{bout}}{2} \right) \quad (15)$$

Method 4:

$$T_b = T \left(\frac{\rho_{bin} + \rho_{bout}}{2} \right) \quad (16)$$

Where T_{bn} ($1 < n < 20$) is the bulk temperature of the middle cross-section of the n th segment; H_b represents the bulk enthalpy; ρ_b represents the density evaluated at bulk temperature; 'T()' is a function of enthalpy (or density) in Eqs. (15) and (16), which can be calculated by NIST Refprop database 9.1.

The whole test procedure for the reference temperature can be described as follows. First, the h_a of 200–1000 mm section at a series of inlet temperatures is acquired from numerical results and formed into a linear interpolation function. Second, for each inlet condition, calculate the h'_a as Eq. (12) in which the h_{an} are calculated by the linear interpolation function of h_a . Finally, evaluate the value of Er as Eq. (10). The comparison result of the four methods is shown in Fig. 5. When the traditional 'Method 1' is used to calculate the reference temperature, the h_a will substantially deviate from h'_a around the pseudo-critical point. Below the pseudo-critical point, it is clear that 'Method 4' makes the h_a more consistent with h'_a . Above the pseudo-critical point, the error trend is relatively complex. It can be noted that 'Method 4' has the slightest

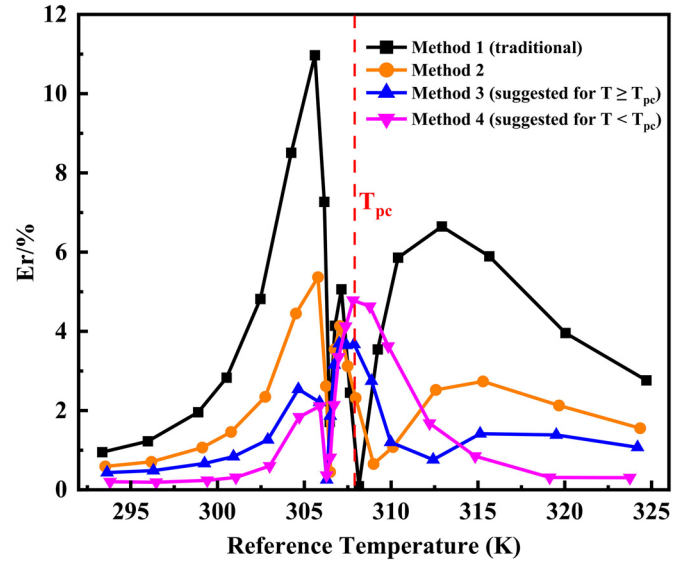


Fig. 5. Comparison of different reference temperature definitions of average HTC.

Table 1

Simulation parameters used in 6.22 and 9.40 mm tubes.

Parameters	Range
Diameter/ mm	6.22/9.40
Pressure/ MPa	7.5/7.8/8.1
Mass flow rate/ $\text{kg}\cdot\text{m}^{-2}\cdot\text{s}^{-1}$	329–1973
Temperature/ $^{\circ}\text{C}$	20–75
Heat flux/ $\text{kW}\cdot\text{m}^{-2}$	10–45

error at high temperature, but it will produce a relatively large error when it is close to the pseudo-critical point. Among them, the deviation of 'Method 3' is moderate at the above pseudo-critical regime.

Therefore, when it is under the pseudo-critical temperature, Eq. (16) is recommended to define the reference temperature of the average HTC. And when it is above the pseudo-critical temperature, Eq. (15) is recommended to define the reference temperature of the average HTC.

Eqs. (17)–(19) can summarize the calculation of HTC.

$$\Delta T = \frac{T_{b1} + T_{b2} + \dots + T_{b5}}{5} - \frac{T_{w1} + T_{w2} + \dots + T_{w5}}{5} \quad (17)$$

$$h(T_b) = \frac{q}{\Delta T} \quad (18)$$

$$\begin{cases} T_b = T \left(\frac{\rho_{bin} + \rho_{bout}}{2} \right), \text{ for } \frac{T_{bin} + T_{bout}}{2} < T_{pc} \\ T_b = T \left(\frac{H_{bin} + H_{bout}}{2} \right), \text{ for } \frac{T_{bin} + T_{bout}}{2} \geq T_{pc} \end{cases} \quad (19)$$

4. Numerical results

In this section, the new reference temperature definition method proposed in this paper will be used to summarize and analyze the average HTC. The simulation parameters for analysis are listed in Table 1. The extrapolated conditions are shown in Table 2. The Re for both small and large diameter corresponds to the case of 6.22 mm.

4.1. Sensitivity analysis of average HTC

The sensitivity analysis of HTC is shown in Fig. 6(a)–(d). Fig. 6(a) shows that the HTC significantly increases with the mass

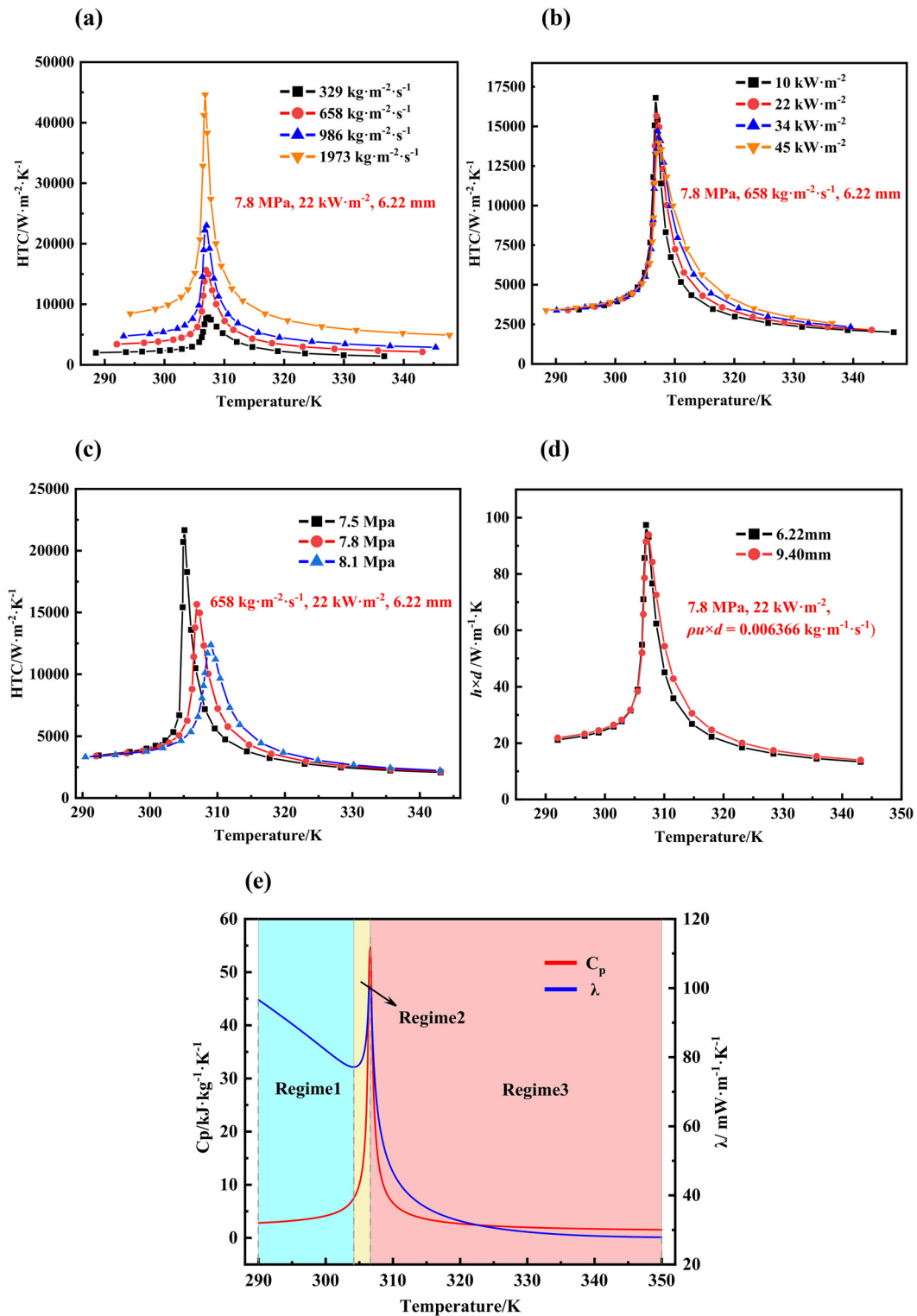


Fig. 6. Sensitivity analysis of average HTC. (a) mass flow rate; (b) heat flux; (c) pressure; (d) diameter, (e) temperature regions of thermal boundary layer.

Table 2
Extrapolated simulation parameters.

Parameters	Range
Diameter/ mm	4.15/14
Pressure/ MPa	7.5/7.8/8.1
Mass flow rate/ $\text{kg}\cdot\text{m}^{-2}\cdot\text{s}^{-1}$	493–1479 for 4.15 mm, 162–487 for 14 mm
Temperature/ $^{\circ}\text{C}$	20–75
Heat flux/ $\text{kW}\cdot\text{m}^{-2}$	13–40

flow rate. The increase in mass flow rate directly leads to an increase in Reynolds number. Therefore, turbulence heat transfer intensifies by increasing the mass flow rate.

The effect of heat flux on HTC is shown in Fig. 6(b), which seems to be complicated. The special effect of heat flux on HTC is due to the characteristics of boundary layer properties in the heat transfer process. As shown in Fig. 6(e), when the boundary layer's temperature is in 'Regime 1', the mainstream bulk temper-

ature is basically below the pseudo-critical point. As heat flux increases, the C_p in the boundary layer decreases but the λ thermal conductivity in the boundary layer increases. The combined factors of these two results keep HTC unchanged [15]. Moreover, when the boundary layer's temperature is in 'Regime 2', the mainstream bulk temperature is almost around the pseudo-critical point. When the heat flux increases, the C_p and the λ in boundary layer decreases, leading to the decrease of HTC. When the boundary layer's temperature is in 'Regime 3', the mainstream bulk temperature is entirely above the pseudo-critical point. With the increase of heat flux, the C_p and the λ in the boundary layer increase, and the heat transfer coefficient rises accordingly. When the temperature of the boundary layer is far away from the pseudo-critical point, the temperature gradient between the boundary layer and the mainstream could be neglected, so the HTC is not affected by heat flux.

The influence of pressure on HTC is shown in Fig. 6(c), mainly due to C_p 's dramatic change. With the increase of pressure, the pseudo-critical point moves to high temperature, and the peak value of C_p reduces and migrates to high temperature, which controls the variation of HTC.

For the influence of pipe diameter, it is more reasonable to keep $\rho u \times d$ as constant (under the same Re) to compare $h \times d$ (Nusselt number). The result is shown in Fig. 6(d). When the diameter increases, the gradient of C_p and λ between the boundary layer and the mainstream increase. Therefore, the influence of tube diameters on HTC is of the identical mechanism to heat flux. Therefore, the influence of pipe diameter needs no further elaboration for simplicity.

4.2. Dimensionless number analysis

The dimensionless numbers' form in Nusselt correlation is essential for predicting heat transfer coefficient. Some further discussion can be found in Supplementary information Chapter 3. In order to develop a Nusselt correlation with both higher accuracy and simplicity, it is necessary to analyze the reference properties in dimensionless numbers.

(1) Reynolds number

The Re is defined by the form of Eq. (20).

$$Re = \frac{du_b \rho_b}{\mu} \quad (20)$$

Where dynamic viscosity can be defined by μ_b, μ_f, μ_w . The subscript of $b, f,$ and w represents bulk, film, and wall properties, respectively.

To determine an applicable form of Re , define \bar{k}_A and $\bar{k}_{A,bound}$ as mean turbulent kinetic energy of flow cross-section and mean turbulent kinetic energy of flow cross-section's boundary layer, respectively. Eqs. (21) and (22) showed them.

$$\bar{K}_A = \frac{\iint_A kdA}{\iint_A dA} \quad (21)$$

$$\bar{K}_{bound} = \frac{\iint_{A_{bound}} kdA}{\iint_{A_{bound}} dA} \quad (22)$$

Where A is the flow cross-section's area; A_{bound} is the flow cross-section's area where the local axial velocity is less than 99% of the bulk axial velocity, which was shown as Eq. (23).

$$A_{bound} = A(u < 0.99u_b) \quad (23)$$

For each simulation case, to avoid the influence of the position taken along the axial of the tube, average values of the middle cross-section of five equally divided segments represent the result, i.e., as Eqs. (24) and (25).

$$\bar{k}_A = \frac{\bar{k}_{A1} + \bar{k}_{A2} + \dots + \bar{k}_{A5}}{5} \quad (24)$$

$$\bar{k}_{bound} = \frac{\bar{k}_{A1,bound} + \bar{k}_{A2,bound} + \dots + \bar{k}_{A5,bound}}{5} \quad (25)$$

Where An is the middle cross-section of the n th segment; An_{bound} is the flow cross-section area occupied by the velocity boundary layer of the n th segment.

The relationship between \bar{k}_{bound} and \bar{k}_A is shown in Fig. 7(a) for pressure of 7.8 MPa, mass flux of 329 kg/(m²•s) and heat flux of 22 kW/m². It can be seen from Fig. 7(a) that the \bar{k}_A is proportional to \bar{k}_{bound} , which means it is sufficient to analyze \bar{k}_A for simplicity.

It can be seen from Fig. 7(b) that the all the three Re increase with the increase of \bar{k}_A , but only Re_b is smoothly rising with \bar{k}_A . In Fig. 7(c), \bar{k}_A, Re_b and Re_f will all go through the fastest-rising position (the dashed line) with the reference temperature increases. Only the Re_b has a same fastest-rising temperature with \bar{k}_A . The Re_w will meet with two fastest-rising temperature (only one dashed line plotted for Re_w because another line will overlap with that of \bar{k}_A and Re_b), which seems to be irrational. Therefore, using Re_b in the definition of Re is reasonable.

(1) Nusselt number

The Nusselt number (Nu) is defined as Eq. (26).

$$Nu = \frac{hd}{\lambda} \quad (26)$$

Where λ can be defined by $\lambda_b, \lambda_f, \lambda_w$.

For no-slip wall surface, there would be Eq. (27).

$$\frac{\partial u}{\partial y} = 0 \quad (27)$$

It represents that the fluid can be regarded as having only heat conduction at the wall surface. Eq. (28) could be derived by combining Newton's law of cooling and Fourier's law of heat conduction.

$$h\Delta T = -\lambda_w \frac{\Delta T}{\Delta y} \quad (28)$$

The form of $\frac{hd}{\lambda}$ can be obtained by transpose the Eq. (28). That is to say, the thermal conductivity at the wall surface has its physical meaning for Nu . Therefore, it is unnatural to use bulk or film temperature to define the thermal conductivity in Nu . The use of bulk temperature to define Nusselt number in the past is only empirically [43].

Moreover, since the properties' radial-gradient are dramatically changed in the heat transfer process near pseudocritical points, the definition of Nusselt in the form of Nu_b or Nu_f will be more deviated from its real physical meaning. Therefore, it is recommended to use Nu_w in the definition of Nu .

(1) Prandtl number

The Prandtl number is defined as Eq. (29).

$$Pr = \frac{\mu C_p}{\lambda} \quad (29)$$

Because it includes three different thermal physical properties, the definition of Pr would be multiple. There are three definitions of dynamic viscosity, i.e., μ_b, μ_f, μ_w . Three definitions of thermal conductivity, i.e., $\lambda_b, \lambda_f, \lambda_w$. Four definitions of isobaric specific heat, i.e., $C_{pb}, C_{pf}, C_{pw}, \bar{C}_p, \bar{C}_p$ is defined as Eq. (30).

$$\bar{C}_p = \frac{H_b - H_w}{T_b - T_w} \quad (30)$$

There will be 36 definitions of Pr . In order to simplify the problem, we can first analyze the thermal conductivity term in the Pr . When the temperature approaches the pseudocritical point, there will be a local extreme value of thermal conductivity. If the thermal conductivity of Pr does not match that of Nu , the HTC may

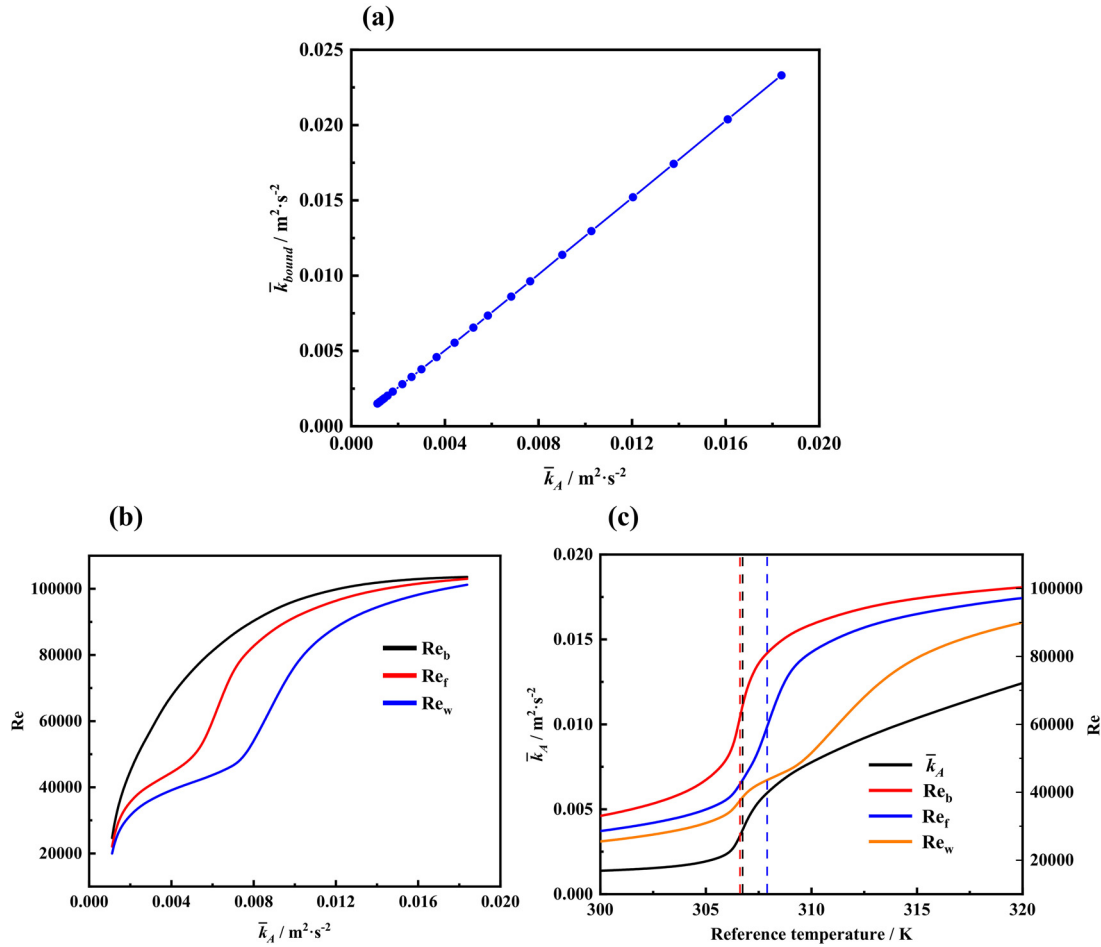


Fig. 7. (a) The relationship between \bar{k}_{bound} and \bar{k}_A ; (b) The relationship between Re and \bar{k}_A ; (c) The relationship between \bar{k}_A and reference temperature.

Table 3

The R^2 of Eq. (31) under different definition of μ and C_p in Pr .

R^2	C_{pb}	C_{pf}	C_{pw}	\bar{C}_p
μ_b	0.9509	0.9405	0.7045	0.9629
μ_f	0.9548	0.9598	0.7563	0.9735
μ_w	0.9667	0.9417	0.7486	0.9529

oscillate near the critical point, which is not in line with reality. Therefore, the λ of Pr should be consistent with the one in Nu , i.e., λ_w .

There are only 12 possible definitions of the Pr . Bazargan and Fraser [44] claimed that the experimental HTC could be agreed with Dittus-Boelter correlation when the reference temperature is reasonably selected between wall temperature and bulk temperature for supercritical fluid heat transfer. Therefore, we believe that the correlation form based on Eq. (31) could also predict the simulation results as well as possible when selecting reasonable μ and C_p in Pr when another two dimensionless numbers were confirmed.

$$Nu_w = aRe_b^b \left(\frac{\mu C_p}{\lambda_w} \right)^c \quad (31)$$

The R^2 value obtained by the correlated results is shown in Table 3. It can be found that when the C_p is consistent but the μ changes, the Pr defined with μ_f can generally obtain a higher R^2 value. The dynamic viscosity in the viscous sublayer contributes to flow resistance, so the definition of μ_f is preferred for variable property fluids [11]. When the μ keeps consistent but the

C_p changes, the C_p defined with \bar{C}_p can generally obtain a higher R^2 value. The heat transfer process in the pseudo-critical regime is like a state of phase-changing [45]. Therefore, \bar{C}_p can be understood as the phase transition's latent heat from the wall to the bulk fluid. That may be why using \bar{C}_p in Pr could get a better-correlated result. In conclusion, it is recommended to use $\frac{\mu_f \bar{C}_p}{\lambda_w}$ to define Pr .

Finally, the property ratio correction term should also be introduced to predict the buoyancy effect reasonably. Based on the numerical result of 6.22 and 9.40 mm, a concise and optimal correlation could be obtained by adding isobaric specific heat and thermal conductivity correction terms as Eq. (32). The correlation is valid for Re of $2.4 \times 10^4 - 6.2 \times 10^5$ and Pr of 1–35 based on numerical results.

$$\frac{hd}{\lambda_w} = 0.0183 \left(\frac{d \rho_b}{\mu_b} \right)^{0.826} \left(\frac{\mu_f \bar{C}_p}{\lambda_w} \right)^{0.44} \left(\frac{C_{pb}}{C_p} \right)^{0.119} \left(\frac{\lambda_f}{\lambda_w} \right)^{0.383} \quad (32)$$

The R^2 of the Eq. (32) for 6.22 and 9.40 mm reached a fantastic value of 0.998. When extrapolated to 4.15 and 14 mm, it also could achieve very high accuracy. Almost all the results (527/528) have relative errors within $\pm 20\%$, which are shown in Fig. 8(a-1)–(a-3).

In addition, it is found that when the Nusselt correlations extrapolated to a larger diameter, the deviation usually increases. This is because the buoyancy effect will be more evident in large diameter tubes even at the same Re . Therefore, the buoyancy effect in larger tubes is different from smaller tubes. More correction terms and a large amount of data should be correlated if we want to get a more accurate correlation. However, Eq. (32) already exhibits enough extrapolation accuracy and a relatively concise form.

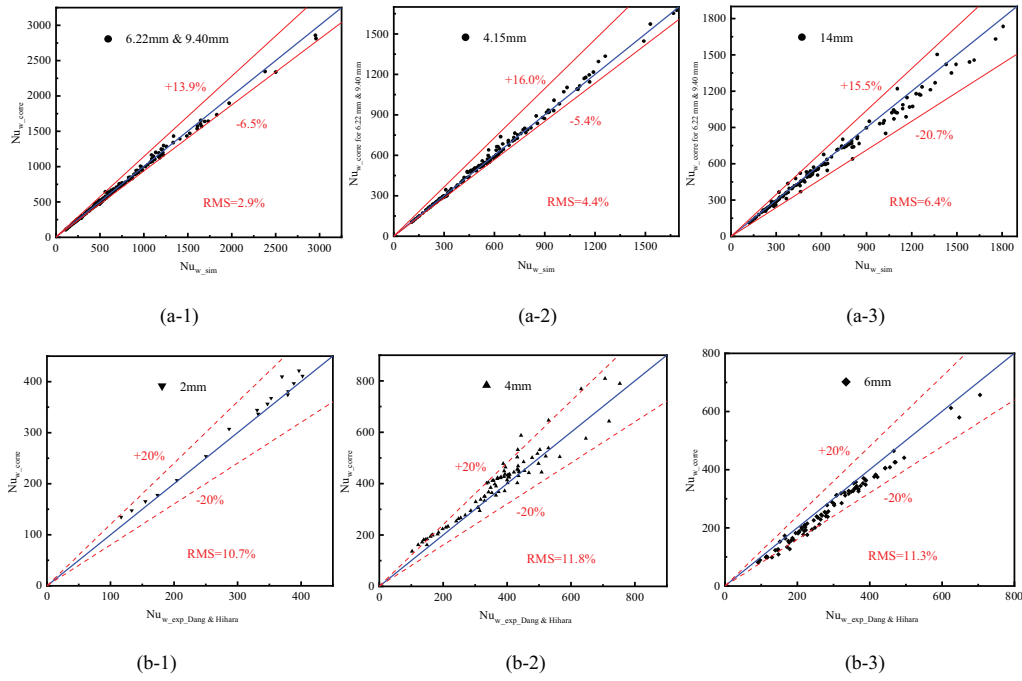


Fig. 8. New correlation compared to the numerical result of (a-1) 6.22 mm and 9.40 mm; (a-2) 4.15 mm; (a-3) 14 mm. And compared to experimental results of Dang and Hihara of: (b-1) 2 mm; (b-2) 4 mm; (b-3) 6 mm.

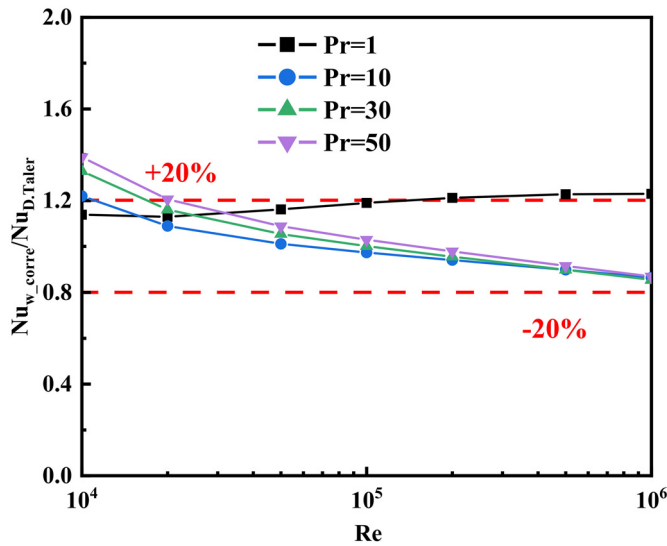


Fig. 9. Comparison of new correlation to Taler [40] correlation for constant property fluids.

The new proposed correlation was compared to the experimental results of Dang and Hihara [11] to verify its applicability. As shown in Fig. 8(b-1)–(b-3), the percentage of experiment data within the relative deviation of $\pm 20\%$ were found to be 100%, 87%, 94% for 2 mm, 4 mm, 6 mm, respectively. The RMS errors were around 11%, which showed good consistency of new correlation and experimental results. In addition, as shown in Fig. 9, the comparison of Eq. (32) to Taler correlation [40] showed good consistency for constant property cases for Re of 2×10^4 – 10^6 and Pr of 1–50, which indicated that the new correlation could be reasonably extrapolated to constant property fluids. Therefore, the correlation proposed in this paper is with good accuracy and universality.

5. Conclusions

In summary, the cooling heat transfer of sCO_2 in a horizontal circular tube is studied through numerical simulation. The main conclusions are as follows:

- (1) The accuracy of eight numerical models for sCO_2 cooling heat transfer is compared. The result shows that the Realizable k - ϵ model with enhanced wall treatment accurately predicts HTC. It can be used as an effective numerical model to study the heat transfer process of sCO_2 .
- (2) A more accurate method of defining the reference temperature of average HTC is proposed for the heat transfer process of variable property fluids, especially at a high heat flux to mass flux ratio. It is recommended to use density-averaged temperature of inlet and outlet below pseudo-critical temperature and to use enthalpy-averaged temperature of inlet and outlet above the pseudo-critical temperature. In this way, the calculated average HTC can be closer to the local HTC to reduce the prediction error of HTC near the pseudo-critical regime.
- (3) For heat transfer correlation of variable property fluids, Nu is recommended to be defined as $\frac{hd}{\lambda_w}$, which is theoretically reasonable. Re is recommended to be defined as $\frac{du\rho_b}{\mu_b}$, which corresponds to the variation rule of turbulence kinetic energy. Pr is recommended to be defined as $\frac{\mu_f \bar{c}_p}{\lambda_w}$, which is numerically proofed and can well reflect the characteristics of heat transfer in the boundary layer.
- (4) Based on numerical simulation, a new Nusselt correlation of sCO_2 turbulent convective cooling heat transfer in the horizontal circular tube is proposed as:

$$\frac{hd}{\lambda_w} = 0.0183 \left(\frac{du\rho_b}{\mu_b} \right)^{0.826} \left(\frac{\mu_f \bar{c}_p}{\lambda_w} \right)^{0.44} \left(\frac{C_{pb}}{\bar{c}_p} \right)^{0.119} \left(\frac{\lambda_f}{\lambda_w} \right)^{0.383}$$

The application range is the diameters of 2–14 mm, the pressure of 7.5–8.1 MPa, the Re of 2.4×10^4 – 6.2×10^5 , the heat flux of 10–45 kW/m^2 . The new correlation exhibited good agreement with

the experimental results of Dang and Hihara and can be extrapolated to fluids with constant properties for the Pr of 1–50 and the Re of 2×10^4 – 10^6 .

Declaration of Competing Interest

The authors declare that they have no known competing financial interests or personal relationships that could have appeared to influence the work reported in this paper.

CRediT authorship contribution statement

Zheng Wang: Conceptualization, Methodology, Investigation, Software, Data curation, Writing – original draft, Writing – review & editing. **Gang Xiao:** Methodology, Writing – review & editing, Project administration, Supervision. **Yafei Liu:** Investigation, Data curation, Writing – review & editing. **Yuxuan Ji:** Investigation, Data curation. **Haoran Xu:** Writing – review & editing, Supervision.

Acknowledgments

The authors gratefully acknowledge the Zhejiang Provincial Natural Science Foundation (NO. LR20E060001) and the Key R&D Program of Zhejiang (2022C01043).

Supplementary materials

Supplementary material associated with this article can be found, in the online version, at doi:10.1016/j.ijheatmasstransfer.2022.122973.

References

- [1] Y. Ahn, S.J. Bae, M. Kim, S.K. Cho, S. Baik, J.I. Lee, J.E. Cha, Review of supercritical CO₂ power cycle technology and current status of research and development, *Nucl. Eng. Technol.* 47 (6) (2015) 647–661.
- [2] Y. Zhang, H. Li, W. Han, W. Bai, Y. Yang, M. Yao, Y. Wang, Improved design of supercritical CO₂ Brayton cycle for coal-fired power plant, *Energy* 155 (2018) 1–14.
- [3] A.K. Sleiti, W.A. Al-Ammari, Energy and exergy analyses of novel supercritical CO₂ Brayton cycles driven by direct oxy-fuel combustor, *Fuel* 294 (2021) 120557.
- [4] K. Wang, Y.L. He, H.H. Zhu, Integration between supercritical CO₂ Brayton cycles and molten salt, lar power towers: a review and a comprehensive comparison of different cycle layouts, *Appl. Energy* 195 (2017) 819–836.
- [5] E. Gümüş, Alternative to ship diesel engine: sCO₂ power cycle, *J. ETA Marit. Sci.* 7 (2) (2019) 117–126.
- [6] E. Açıkkalp, Ecologic and sustainable objective thermodynamic evaluation of molten carbonate fuel cell–supercritical CO₂ Brayton cycle hybrid system, *Int. J. Hydrog. Energy* 42 (9) (2017) 6272–6280.
- [7] E.M. Clementoni, T.L. Cox, Comparison of carbon dioxide property measurements for an operating supercritical brayton cycle to the refprop physical property database, in: *Proceedings of the ASME Turbo Expo 2014: Turbine Technical Conference and Exposition*, 2014.
- [8] B.S. Petukhov, Heat transfer and friction in turbulent pipe flow with variable physical properties, *Adv. Heat Transf.* 6 (1970) 503–564.
- [9] S.H. Yoon, J.H. Kim, Y.W. Hwang, M.S. Kim, K. Min, Y. Kim, Heat transfer and pressure drop characteristics during the in-tube cooling process of carbon dioxide in the supercritical region, *Int. J. Refrig.* 26 (8) (2003) 857–864.
- [10] S.M. Liao, T.S. Zhao, Measurements of heat transfer coefficients from supercritical carbon dioxide flowing in horizontal mini/micro channels, *J. Heat Transf.* 124 (3) (2002) 413–420.
- [11] C. Dang, E. Hihara, In-tube cooling heat transfer of supercritical carbon dioxide. Part 1. Experimental measurement, *Int. J. Refrig.* 27 (7) (2004) 736–747.
- [12] X.L. Huai, S. Koyama, T.S. Zhao, An experimental study of flow and heat transfer of supercritical carbon dioxide in multi-port mini channels under cooling conditions, *Chem. Eng. Sci.* 60 (12) (2005) 3337–3345.
- [13] H.K. Oh, C.H. Son, New correlation to predict the heat transfer coefficient in-tube cooling of supercritical CO₂ in horizontal macro-tubes, *Exp. Therm. Fluid Sci.* 34 (8) (2010) 1230–1241.
- [14] X. Fang, Y. Xu, Modified heat transfer equation for in-tube supercritical CO₂ cooling, *Appl. Therm. Eng.* 31 (14–15) (2011) 3036–3042.
- [15] J. Wang, Z. Guan, H. Gurgenci, A. Veeraragavan, X. Kang, K. Hooman, A computationally derived heat transfer correlation for in-tube cooling turbulent supercritical CO₂, *Int. J. Therm. Sci.* 138 (2019) 190–205.
- [16] Z.B. Liu, Y.L. He, Y.F. Yang, J.Y. Fei, Experimental study on heat transfer and pressure drop of supercritical CO₂ cooled in a large tube, *Appl. Therm. Eng.* 70 (1) (2014) 307–315.
- [17] A. Wahl, R. Mertz, E. Laurien, J. Starflinger, Heat transfer correlation for sCO₂ cooling in a 2 mm tube, *J. Supercrit. Fluids* 173 (2021) 105221.
- [18] K. Mori, J. Onishi, H. Shimaoka, S. Nakanishi, H. Kimoto, Cooling heat transfer characteristics of CO₂ and CO₂–oil mixtures at supercritical pressure conditions, *Trans. Jpn. Soc. Refrig. Air Cond. Eng.* 20 (3) (2003) 407–412.
- [19] C. Dang, K. Iino, K. Fukuoka, E. Hihara, Effect of lubricating oil on cooling heat transfer of supercritical carbon dioxide, *Int. J. Refrig.* 30 (4) (2007) 724–731.
- [20] C.R. Zhao, P.X. Jiang, Y.W. Zhang, Flow and convection heat transfer characteristics of CO₂ mixed with lubricating oil at super-critical pressures in small tube during cooling, *Int. J. Refrig.* 34 (1) (2011) 29–39.
- [21] C.R. Zhao, Z. Zhang, P.X. Jiang, Predictions of In-tube cooling heat transfer coefficients and pressure drops of CO₂ and lubricating oil mixture at supercritical pressures, *Heat Transf. Eng.* 39 (16) (2017) 1437–1449.
- [22] C. Dang, E. Hihara, In-tube cooling heat transfer of supercritical carbon dioxide. Part 2. Comparison of numerical calculation with different turbulence models, *Int. J. Refrig.* 27 (7) (2004) 748–760.
- [23] P.X. Jiang, Y. Zhang, R.F. Shi, Experimental and numerical investigation of convection heat transfer of CO₂ at supercritical pressures in a vertical mini-tube, *Int. J. Heat Mass Transf.* 51 (11) (2008) 3052–3056.
- [24] K. Wang, X. Xu, Y. Wu, C. Dang, Numerical investigation on heat transfer of supercritical CO₂ in heated helically coiled tubes, *J. Supercrit. Fluids* 99 (2015) 112–120.
- [25] H. Zhang, J. Guo, X. Huai, X. Cui, Thermodynamic performance analysis of supercritical pressure CO₂ in tubes, *Int. J. Therm. Sci.* 146 (2019) 106102.
- [26] H. Zhang, J. Guo, X. Cui, X. Huai, Heat transfer performance of supercritical pressure CO₂ in a non-uniformly heated horizontal tube, *Int. J. Heat Mass Transf.* 155 (2020) 119748.
- [27] J. Guo, M. Xiang, H. Zhang, X. Huai, K. Cheng, X. Cui, Thermal-hydraulic characteristics of supercritical pressure CO₂ in vertical tubes under cooling and heating conditions, *Energy* 170 (2019) 1067–1081.
- [28] Z. Du, W. Lin, A. Gu, Numerical investigation of cooling heat transfer to supercritical CO₂ in a horizontal circular tube, *J. Supercrit. Fluids* 55 (1) (2010) 116–121.
- [29] L. Diao, Y. Chen, Y. Li, Nonuniform heat transfer of supercritical pressure carbon dioxide under turbulent cooling condition in circular tubes at various inclination angles, *Nucl. Eng. Des.* 352 (2019) 110153.
- [30] Z. Zhao, B. Yuan, W. Du, Assessment and modification of buoyancy criteria for supercritical pressure CO₂ convection heat transfer in a horizontal tube, *Appl. Therm. Eng.* 169 (2020) 114808.
- [31] J. Wang, Z. Guan, H. Gurgenci, A. Veeraragavan, X. Kang, Y. Sun, K. Hooman, Numerical study on cooling heat transfer of turbulent supercritical CO₂ in large horizontal tubes, *Int. J. Heat Mass Transf.* 126 (2018) 1002–1019.
- [32] P.X. Jiang, C.R. Zhao, R.F. Shi, Y. Chen, W. Ambrosini, Experimental and numerical study of convection heat transfer of CO₂ at super-critical pressures during cooling in small vertical tube, *Int. J. Heat Mass Transf.* 52 (21–22) (2009) 4748–4756.
- [33] R.W. Allen, E.R.G. Eckert, Friction and heat-transfer measurements to turbulent pipe flow of water ($Pr=7$ and 8) at uniform wall heat flux, *J. Heat Transf.* 86 (3) (1964) 301–310.
- [34] G.W. Zhang, P. Hu, L.X. Chen, M.H. Liu, Experimental and simulation investigation on heat transfer characteristics of in-tube supercritical CO₂ cooling flow, *Appl. Therm. Eng.* 143 (2018) 1101–1113.
- [35] E.W. Lemmon, M.L. Huber, M.O. McLinden, NIST Standard Reference Database 23: Reference Fluid Thermodynamic and Transport Properties-REFPROP, Version 9.1, Natl. Std. Ref. Data Series (NIST NSRDS), National Institute of Standards and Technology, Gaithersburg, MD, 2013 [online], https://tsapps.nist.gov/publication/get_pdf.cfm?pub_id=912382 (Accessed May 3, 2022).
- [36] R. Abid, Evaluation of two-equation turbulence models for predicting transitional flows, *Int. J. Eng. Sci.* 31 (6) (1993) 831–840.
- [37] K. Abe, T. Kondoh, Y. Nagano, A new turbulence model for predicting fluid flow and heat transfer in separating and reattaching flows—I. Flow field calculations, *Int. J. Heat Mass Transf.* 37 (1) (1994) 139–151.
- [38] K.C. Chang, W.D. Hsieh, C.S. Chen, A modified low-Reynolds-number turbulence model applicable to recirculating flow in pipe expansion, *J. Fluids Eng.* 117 (3) (1995) 417–423.
- [39] B.E. Launder, B.I. Sharma, Application of the energy-dissipation model of turbulence to the calculation of flow near a spinning disc, *Lett. Heat Mass Transf.* 1 (2) (1974) 131–137.
- [40] D. Taler, A new heat transfer correlation for transition and turbulent fluid flow in tubes, *Int. J. Therm. Sci.* 108 (2016) 108–122.
- [41] B.O. Hasan, Heat transfer analysis in thermal entrance region under turbulent flow conditions, *Asia Pac. J. Chem. Eng.* 8 (4) (2013) 578–592.
- [42] R.H. Notter, C.A. Sleicher, A solution to the turbulent Graetz problem—III fully developed and entry region heat transfer rates, *Chem. Eng. Sci.* 27 (11) (1972) 2073–2093.
- [43] S.W. Churchill, Comprehensive correlating equations for heat, mass and momentum transfer in fully developed flow in smooth tubes, *Ind. Eng. Chem. Fundam.* 16 (1) (1977) 109–116.
- [44] M. Bazargan, D. Fraser, Heat transfer to supercritical water in a horizontal pipe: modeling, new empirical correlation, and comparison against experimental data, *J. Heat Transf.* 131 (6) (2009) 061702.
- [45] D.T. Banuti, Crossing the widom-line – supercritical pseudo-boiling, *J. Supercrit. Fluids* 98 (2015) 12–16.